ISSN 1070-3284, Russian Journal of Coordination Chemistry, 2023, Vol. 49, No. 2, pp. 86–96. © Pleiades Publishing, Ltd., 2023.
Russian Text © The Author(s), 2023, published in Koordinatsionnaya Khimiya, 2023, Vol. 49, No. 2, pp. 111–121.

Cobalt(II) and Copper(II) Complexes with New Ditopic Ligand 5-(2-(1*H*-Tetrazol-1-yl)phenyl)-1*H*-tetrazole: Synthesis and Properties

L. G. Lavrenova[a, *], E. Yu. Grigor'ev[b], V. Yu. Komarov[a], L. A. Glinskaya[a], A. N. Lavrov[a, c], and Yu. V. Grigor'ev[b]

[a] *Nikolaev Institute of Inorganic Chemistry, Siberian Branch, Russian Academy of Sciences, Novosibirsk, Russia*
[b] *Institute of Physicochemical Problems, Belarussian State University, Minsk, Belarus*
[c] *Novosibirsk National Research State University, Novosibirsk, Russia*
**e-mail: ludm@niic.nsc.ru*

Received July 6, 2022; revised August 30, 2022; accepted September 8, 2022

Abstract—A procedure for the synthesis of the new ditopic ligand combining in the structure 1- and 5-substituted tetrazolyl cycles, 5-(2-(1*H*-tetrazol-1-yl)phenyl)-1*H*-tetrazole (HL), is developed. The coordination compounds of Co(II) and Cu(II) halides $[Co(HL)_2Cl_2]$, $[Cu(HL)_2Cl_2]$, $[Cu(HL)_2Br_2]$, and $[CuL_2(H_2O)]_n$ based on ligand HL are synthesized. The complexes are studied by elemental analysis, diffuse reflectance spectroscopy, IR spectroscopy, X-ray diffraction (XRD), and static magnetic susceptibility. The crystal structure of the molecular coordination polymer $[CuL_2(H_2O)]_n$ is determined by XRD (CIF file CCDC no. 2127210). The temperature and field dependences of the magnetization show that the magnetic properties of the synthesized Cu(II) complexes are due to exchange interactions in one-dimensional chains of the copper ions ($S = 1/2$). For complex $[Cu(HL)_2Br_2]$, the parameters are shifted toward the enhancement of the antiferromagnetic interaction compared to the analog containing the chloride ion.

Keywords: synthesis, 5-(2-(1*H*-tetrazol-1-yl)phenyl)-1*H*-tetrazole, cobalt(II) and copper(II) complexes, XRD, diffuse reflectance spectroscopy, IR spectroscopy, magnetic activity

DOI: 10.1134/S1070328422700294

INTRODUCTION

The recent decades were marked by an increased number of scientific articles devoted to the synthesis and studies of the structures, properties, and prospects of using complexes of tetrazole derivatives, which is favored by the synthetic availability of the latter and the development of modern high-precision physicochemical and computational investigation methods. Owing to four coordinatively active nitrogen atoms in the tetrazole cycle, the tetrazole derivatives make it possible to synthesize a broad range of metal complexes with a number of specific properties. These complexes are interesting as energetic materials [1], chemosensors [2, 3], gas sorbents [4], catalysts [5], and units for nonlinear optics [6] and light emitting [7–9] and dielectric [10] devices. The structures of more than 1500 crystal structures of compounds of this series included into the Cambridge Structural Database have been solved and described to date. Particular aspects of the coordination chemistry of tetrazoles were reviewed [11–16]. The coordination chemistry of 1- and 5-substituted tetrazoles with 3*d*-metal salts is studied in most detail. However, published data on the complexes of tetrazole derivatives containing simultaneously 1- and 5-substituted tetrazolyl fragments are lacking.

Continuing our studies in the field of the synthetic and coordination chemistry of the tetrazole derivatives [17–22], we synthesized the first representative of ditopic tetrazole-containing ligands combining in the structure both 1- and 5-substituted tetrazole cycles, 5-(2-(1*H*-tetrazol-1-yl)phenyl)-1*H*-tetrazole (HL), and HL-based cobalt(II) and copper(II) complexes.

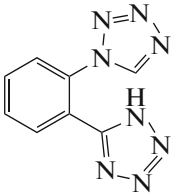

HL

EXPERIMENTAL

Commercially available solvents and reagents were used as received for synthetic purposes.

Synthesis of 5-(2-(1*H*-tetrazol-1-yl)phenyl)-1*H*-tetrazole (HL). Protocol (1). 2-Aminobenzonitrile (0.1 mol, 11.8 g) was added at room temperature to a

stirred mixture of NaN_3 (0.12 mol, 7.8 g) and $Et_3N{\cdot}HCl$ (0.12 mol, 16.5 g) in toluene (100 mL). The reaction mixture was stirred at 100°C for 30 h. After the end of the process, the reaction mixture was evaporated in vacuo, the residue was dissolved in H_2O (100 mL), NaOH (0.15 mol, 6 g) was added, and the resulting solution was evaporated in vacuo. The residue was dissolved in H_2O (150 mL) and filtered. The filtrate was acidified with HCl to pH ~5–6. The formed precipitate was filtered off, washed with water on the filter, and dried at room temperature in vacuo. A yellow amorphous powder of 2-(1*H*-tetrazol-5-yl)aniline with T_m ~ 125°C was obtained in a yield of 16.2 g. After recrystallization from water, the yield of HL as yellow needle-like crystals (T_m = 143–145°C) was 14.5 g (90%).

^{1}H NMR (DMSO-d_6; δ, ppm): 3.36 s (2H, NH_2), 6.66–7.72 m (4H, Ph). ^{13}C NMR (δ, ppm): 104.5, 115.5, 116.3, 127.9, 131.8, 147.4, 154.8 (Tz). IR (ν, cm^{-1}): 3403 s, 3123 s, 3060 s, 3032 s, 2992 s, 2912 s, 2854 s, 2790 s, 2767 s, 2655 s, 2567 s, 2509 m, 1959 w, 1928 w, 1844 w, 1809 w, 1648 m, 1608 s, 1555 s, 1492 s, 1464 s, 1411 m, 1370 w, 1328 w, 1300 m, 1252 m, 1152 s, 1105 m, 1088 m, 1064 s, 1041 m, 991 s, 953 m, 925 m, 864 s, 839 m, 780 m, 749 s, 697 s, 665 s, 571 s, 494 m, 469 m.

For $C_7H_7N_5$ (*FW* = 161.2)			
Anal. calcd., %	C, 52.2	H, 4.4	N, 43.5
Found, %	C, 52.1	H, 4.3	N, 43.1

Protocol (2). A mixture of 2-(1*H*-tetrazol-5-yl)aniline (0.02 mol, 3.22 g), triethyl orthoformate (0.06 mol, 9.66 g), and NaN_3 (0.022 mol, 1.43 g) in glacial acetic acid (0.18 mol, 10.8 g) was stirred at 100°C for 3 h. After the end of the process, the reaction mixture was poured with stirring into H_2O (150 mL), concentrated HCl (5 mL) was added, and the formed precipitate was filtered off. The product was washed with water on the filter and dried at 70°C in vacuo. The yield of HL as a colorless amorphous powder with T_m = 162–165°C (with decomp.) was 3.3 g (77.1%). ^{1}H NMR (DMSO-d_6; δ, ppm): 7.86–8.15 m (4H, Ph), 9.79 s (1H, CH_{Tz}). ^{13}C NMR (δ, ppm): 128.1, 130.3, 131.5, 131.6, 131.9, 145.0, 149.6. IR (ν, cm^{-1}): 3435 s, 3364 s, 3300 s, 3257 s, 3108 m, 3079 m, 1980 m, 1943 m, 1798 w, 1750 w, 1696 w, 1673 w, 1615 w, 1573 m, 1502 m, 1473 m, 1428 w, 1402 w, 1376 w, 1309 w, 1279 w, 1244 w, 1208 s, 1173 m, 1156 s, 1121 m, 1083 s, 1044 s, 1026 s, 977 s, 901 s, 789 w, 751 s, 713 s, 672 s, 645 s, 585 s, 533 s, 473 s, 446 m.

For $C_8H_6N_8$ (*FW* = 214.2)			
Anal. calcd., %	C, 44.9	H, 2.8	N, 52.3
Found, %	C, 44.5	H, 2.8	N, 52.0

Synthesis of $[Co(HL)_2Cl_2]$ (I). Weighed samples of $CoCl_2{\cdot}6H_2O$ (0.5 mmol, 0.12 g) and HL (1 mmol, 0.21 g) were dissolved separately on heating in ethanol (6 mL), and the resulting solutions were mixed together. A finely crystalline green precipitate was formed after a solvent excess was removed and the solution was cooled in a crystallizer with ice. The precipitate was filtered off, washed two times with small portions of ethanol, and dried in air. The yield was 0.28 g (57%).

For $C_{16}H_{12}N_{16}Cl_2Co$			
Anal. calcd., %	C, 34.4	H, 2.2	N, 40.1
Found, %	C, 34.2	H, 2.4	N, 39.1

Synthesis of $[Cu(HL)_2Cl_2]$ (II). Weighed samples of $CuCl_2{\cdot}2H_2O$ (0.5 mmol, 0.09 g) and HL (1.5 mmol, 0.32 g) were dissolved separately on heating in ethanol (15 mL), and the resulting solutions were mixed together. The formed blue solution was evaporated to 1/3 of the initial volume and cooled in a crystallizer with ice until the formation of a blue precipitate. The precipitate was filtered off, washed two times with small portions of ethanol, and dried in air. The yield was 0.26 g (92%).

For $C_{16}H_{12}N_{16}Cl_2Cu$			
Anal. calcd., %	C, 34.1	H, 2.2	N, 39.8
Found, %	C, 34.2	H, 2.5	N, 39.4

Synthesis of $[Cu(HL)_2Br_2]$ (III). Weighed samples of $CuBr_2$ (0.5 mmol, 0.11 g) and HL (1 mmol, 0.21 g) were dissolved separately on heating in ethanol (6 mL), and the resulting solutions were mixed together. A brown precipitate of the complex was formed after a solvent excess was removed and the solution was cooled in a crystallizer with ice. The precipitate was filtered off, washed two times with small portions of ethanol, and dried in air. The yield was 0.17 g (52%).

For $C_{16}H_{12}N_{16}Br_2Cu$			
Anal. calcd., %	C, 29.5	H, 1.9	N, 34.4
Found, %	C, 29.7	H, 1.7	N, 33.9

Synthesis of $[CuL_2(H_2O)]_n$ (IV). Single crystals of complex $[CuL_2(H_2O)]_n$ suitable for XRD were prepared in an H-shaped tube by the interaction of ethanolic solutions of $CuCl_2$ and HL taken in the stoichiometric ratio.

Elemental analysis was carried out at the Analytical Laboratory of the Nikolaev Institute of Inorganic Chemistry (Siberian Branch, Russian Academy of Sciences) on a EUROEA 3000 instrument (EuroVector, Italy).

Table 1. Crystallographic characteristics and experimental and structure refinement details for complex $[CuL_2(H_2O)]_n$

Parameter	Value
Empirical formula	$C_{16}H_{12}N_{16}OCu$
FW	507.96
Crystal system	Orthorhombic
Space group	$Pna2_1$
a, Å	9.4669(4)
b, Å	9.3012(3)
c, Å	22.8230(9)
V, Å^3	2009.65(13)
Z; ρ_{calc}, mg/cm^3	4; 1.679
μ, mm^{-1}	1.138
Crystal sizes, mm	0.1 × 0.03 × 0.03
Scan range over θ, deg	4.73–52.74
Number of measured reflections	19360
Number of independent reflections	4099
R_{int}	0.075
Number of reflections with $I > 2\sigma(I)$	3375
Number of refined parameters	308
GOOF for F^2	1.029
R factor, $I > 2\sigma(I)$	
R_1	0.0421
wR_2	0.0828
R factor (for all I_{hkl})	
R_1	0.0580
wR_2	0.0904
Residual electron density (max/min) e/Å^3	0.40/–0.40
Absolute structure parameter	–0.004(12)

Diffraction studies of polycrystalline samples were carried out on a Shimadzu XRD 7000 diffractometer (CuK_α radiation, Ni filter, Mythen2 R 1K complementary metal-oxide-semiconductor (CMOS) sensor) at room temperature. The samples were triturated in heptane and supported on the polished side of a glass cell or without triturating were packed into a hollow of a low-background single-crystal Si cell. Recording was carried out in a high-precision mode in the 5°–60° angle range at an integration time of 0.014° and the total acquisition time at least 20 s/point. The obtained diffraction patterns show that the L phase and observed impurities of phases with different L contents are absent from the samples.

XRD was conducted using a standard procedure on a Bruker D8 Venture automated three-circle diffractometer (MoK_α IμS3.0 with focusing using Incoatec HELIOS multilayer Montel mirrors, PHOTON III two-coordinate CMOS sensor, 150 K nitrogen thermostat). Integration was performed and an absorption correction was applied by equivalent reflection intensities using the APEX3 software [23]. The structure of complex **IV** was solved using the SHELXT program

Table 2. Selected interatomic distances (Å) and bond angles (deg) in the structure of complex $[CuL_2(H_2O)]_n$ *

Bond	*d*, Å	Bond	*d*, Å
Cu(1)–O(1)	1.988(5)	N(17)–N(16)	1.311(6)
Cu(1)–N(26)	1.962(5)	N(15)–C(18)	1.345(7)
Cu(1)–N(16)	1.975(5)	N(15)–N(16)	1.336(7)
Cu(1)–N(18)[1]	2.065(5)	N(26)–N(27)	1.325(7)
Cu(1)–N(22)[2]	2.157(5)	N(27)–N(28)	1.355(7)
N(18)–N(17)	1.337(6)	N(28)–C(28)	1.331(8)
N(18)–C(18)	1.327(7)	N(25)–C(28)	1.339(7)
Angle	ω, deg	Angle	ω, deg
O(1)Cu(1)N(18)[1]	131.4(2)	N(26)Cu(1)N(16)	177.2(2)
N(26)Cu(1)N(18)[1]	89.8(2)	N(22)[2]Cu(1)N(18)[1]	102.7(2)
N(26)Cu(1)O(1)	89.5(2)	N(22)[2]Cu(1)O(1)	125.9(2)
N(16)Cu(1)N(18)[1]	92.8(2)	N(22)[2]Cu(1)N(26)	91.2(2)
N(16)Cu(1)O(1)	89.3(2)	N(22)[2]Cu(1)N(16)	87.5(2)

* Symmetry codes: [1] $1/2 + x, 1/2 - y, z$; [2] $-1/2 + x, 1/2 - y, z$.

[24] and refined by full-matrix least squares for F^2 in the anisotropic approximation for all non-hydrogen atoms in SHELXL [25] using OLEX2 [26]. The hydrogen atoms of the ligand were localized from the difference Fourier synthesis and refined by the riding model in the isotropic approximation with fixed $U_{iso}(H)$ equal to $1.5U_{eq}(O)$ and $1.2U_{eq}(C)$, respectively. The correctness of positions of the hydrogen atoms of the water molecules was confirmed by their arrangement near the hydrogen bond lines. The main crystallographic data and refinement details are given in Table 1. Selected interatomic distances and bond angles for $[CuL_2(H_2O)]_n$ are listed in Table 2.

The coordinates of atoms and thermal parameters for complex $[CuL_2(H_2O)]_n$ were deposited with the Cambridge Crystallographic Data Centre (CIF file CCDC no. 2127210; https://www.ccdc.cam.ac.uk/structures/).

NMR spectra were detected on a Bruker Avance 500 spectrometer at the working frequencies 500 MHz (^1H) and 150 MHz (^{13}C) using $(CD_3)_2SO_4$ as the solvent.

IR absorption spectra were recorded on an IR Thermo Avatar 330 spectrometer (Nicolet) in a frequency range of 4000–400 cm^{-1} for the ligand and on Scimitar FTS 2000 and Vertex 80 spectrometers in a frequency range of 4000–100 cm^{-1} for the complexes. Samples of the complexes were prepared as suspensions in Nujol, fluorinated oil, and polyethylene. The Kubelka–Munk diffuse reflectance spectra were measured on a UV-3101 PC scanning spectrophotometer (Shimadzu) at room temperature.

The magnetic properties of the polycrystalline samples were studied on an MPMS-XL SQUID magnetometer (Quantum Design) in a temperature range of 1.77–300 K and in the magnetic field range $H = 0$–10 kOe. To determine the paramagnetic component of the molar magnetic susceptibility $\chi_p(T)$, the contributions from Larmor diamagnetism (χ_d) and ferromagnetism of microimpurities (χ_F) were subtracted from the measured values of the total molar susceptibility $\chi = M/H$ (M is magnetization): $\chi_p(T,H) = \chi(T,H) - \chi_d - \chi_F(T,H)$. The temperature-independent contribution χ_d was calculated according to Pascal's additive scheme. The field dependences $M(H)$ were measured to determine the ferromagnetic contribution χ_F.

RESULTS AND DISCUSSION

The [3 + 2] cycloaddition of the azide ion to alkyl or aryl cyanides is known to be a convenient method for the synthesis of C-substituted tetrazoles [27], and N(1)-substituted tetrazoles can be synthesized in high yields by the heterocyclization of primary amines with triethyl orthoformate and sodium azide [28, 29]. We accomplished these approaches to synthesize 5-(2-(1*H*-tetrazol-1-yl)phenyl)-1*H*-tetrazole (HL) (Scheme 1).

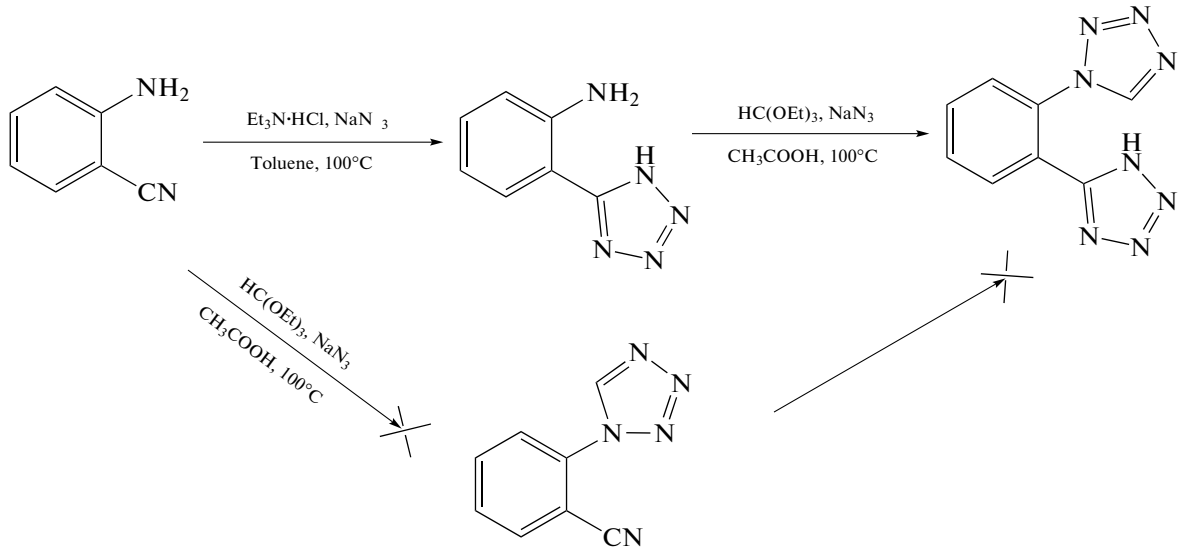

Scheme 1.

An attempt to synthesize ligand HL by the primary heterocyclization of the amino group of 2-aminobenzonitrile with the formation of intermediate 2-(1*H*-tetrazol-1-yl)benzonitrile failed, because this reaction affords a poorly separable mixture of tetrazole-containing products and, hence, it seems impossible to isolate 2-(1*H*-tetrazol-1-yl)benzonitrile in the individual state from this mixture in any appropriate yield.

Complexes **I**–**III** were isolated from aqueous-ethanol solutions at different metal to ligand ratios. The ratios were selected experimentally to obtain phases of a certain composition. The XRD data showed the crystalline character of synthesized complexes **I**–**III**, but there are no isostructural complexes among them. During the crystallization of complex **II** at room temperature, ligand HL loses the hydrogen ion affording crystals of complex **IV** suitable for XRD. All synthesized phases are stable in air for a long time.

The crystal structure of $[CuL_2(H_2O)]_n$ (**IV**) consists of one-dimensional chains of the molecular coordination polymer (Fig. 1). Two adjacent copper(II) ions are linked by two bidentate-bridging ligands L performing different ligand functions. One of the ligands is coordinated by the nitrogen atoms of different tetrazole cycles (structural numeration of atoms: N(16), N(18A)), and the second ligand is coordinated by the nitrogen atoms of the tetrazole cycle linked with the phenyl fragment of the C atom (structural numeration of atoms: N(22), N(26A), respectively). The oxygen atom of the water molecule additionally coordinates to each copper(II) ion. The coordination polyhedron of the copper(II) ion is a trigonal bipyramid $\{CuN_4O\}$ with the N(18A), N(22B), O(1) and N(18C), N(22), O(1A) atoms (bond lengths 2.065(5), 2.157(5), and 1.988(4) Å) in the equatorial plane (deviation of the Cu(1) ion from the equatorial plane is 0.004 Å) and the N(16) and N(26) atoms (bond lengths 1.975(5) and 1.962(5) Å) in the apical positions. The angles of the Cu(1)–N(16) and Cu(1)–N(26) bonds with the equatorial plane are ~90°.

The polymer chains extending along the *a* axis are shown in Fig. 2. Two such chains fall onto one unit cell. The chains are zigzag in the [001] direction (Fig. 3). The distance between two closest Cu(II) ions in the chain is 5.686(1) Å, and the Cu(1)Cu(1)'Cu(1)" angle is 112.8°. Interestingly, each coordinated water molecule forms both the interchain hydrogen bond with the N(28) atom (O(1)...N(28) 2.686(1) Å, angle O(1)H(1B)N(28) 166.5°) and intrachain hydrogen bond with the N(12) atom of the uncoordinated tetrazole ring (O(1)...N(12) 2.742(1)Å, O(1)H(1A)N(12) 133.8°) (Fig. 3). Cycles L are unfolded to each other almost at an angle of ~90° (88.7°). The N(16)Cu(1)N(18) angle is 92.8°.

The main absorption bands and the corresponding vibrational frequencies of ligand HL and complexes **I**–**III** are given in Table 3. The bands characteristic of ν(NH) vibrations are observed in a range of 3400–3100 cm^{-1}, and the range from 3100 to 2800 cm^{-1} contains bands corresponding to ν(CH) vibrations. The bands corresponding to stretching and bending vibrations of the tetrazole and phenyl rings are observed in a range of 1630–1400 cm^{-1}. The number and positions of bands change in the range of ring vibrations upon complex formation, indicating the coordination of the nitrogen atoms of the tetrazole cycles to the metal ions. The low-frequency spectral range exhibits the bands of stretching vibrations ν(M–N) and ν(M–Hal) (Table 3). This indicates the coordination of the ligands to the metal ions by the nitrogen atoms of the tetrazole ring and halide ions.

The diffuse reflectance spectra of complex $[Co(HL)_2Cl_2]$ contains three bands of *d*–*d* transitions: the band at 20000 cm^{-1} (ν_3) and the split band at

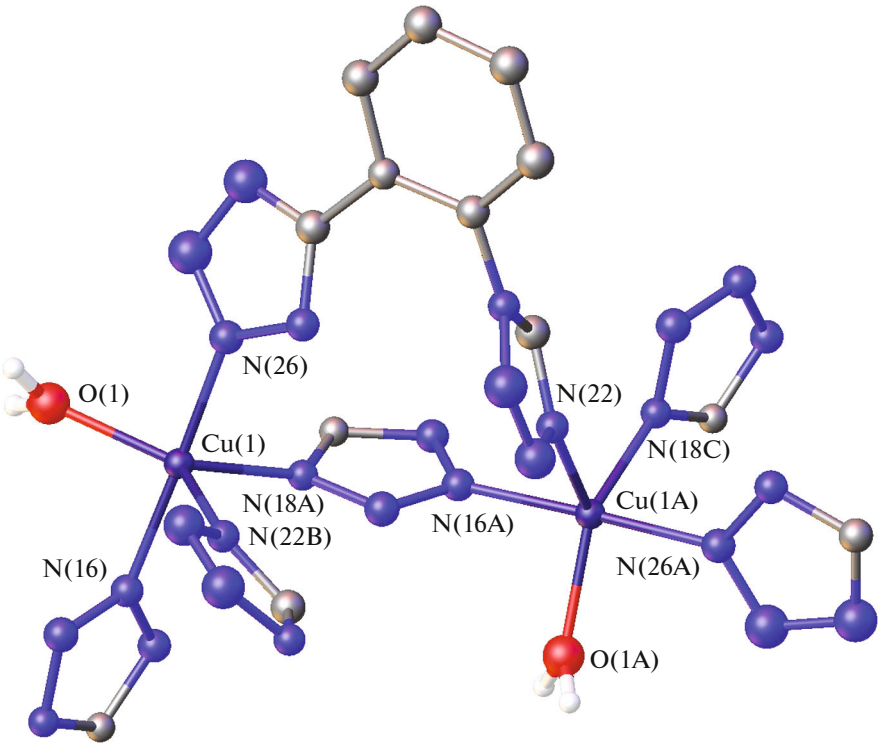

Fig. 1. Structure of the molecule of complex $[CuL_2(H_2O)]_n$. Hydrogen atoms and some tetrazole and phenyl cycles are omitted for clarity.

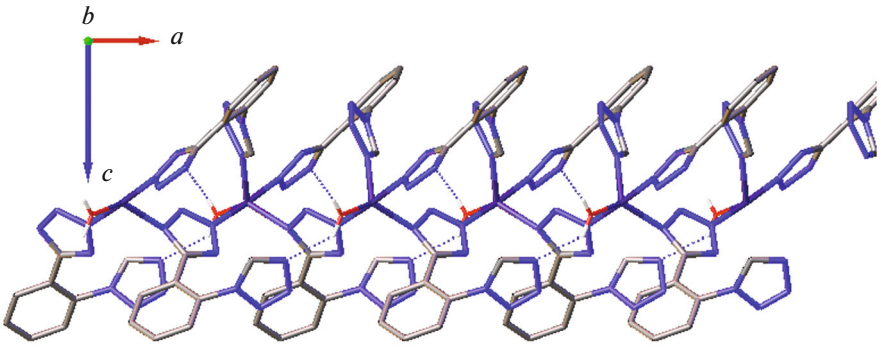

Fig. 2. Polymer chains of molecules of complex $[CuL_2(H_2O)]_n$ in the crystal structure projected onto the (010) plane.

16807, 15873, and 15152 cm^{-1} (ν_2) and 7692 cm^{-1} (ν_1). The numbers and positions of the *d*–*d*-transition bands in the $Co(HL)_2Cl_2$ complex indicate that the compound has the octahedral coordination polyhedron. The splitting parameter 10 Dq for this complex was calculated from the condition $\nu_1 = 8.8$ Dq and is equal to 8740 cm^{-1}. The obtained value of the splitting parameter indicates the coordination of the chloride ions (along with the nitrogen atoms of the ligands) to the Co(II) ion. The diffuse reflectance spectra of the copper(II) complexes contain one broad band, the assignment of which is difficult.

The measured magnetic susceptibility of the $[Co(HL)_2Cl_2]$ complex demonstrates a smooth paramagnetic growth on cooling in the whole temperature range from 300 to 1.77 K (Fig. 4a). Formally, the temperature dependence $\chi_p(T)$ in a range of 50–300 K can be described by the Curie–Weiss law $\chi_p(T) = N_A\mu_{eff}^2/3k_B(T - \theta)$, where N_A and k_B are Avogadro's number and Boltzmann constant with the effective magnetic moment $\mu_{eff} \approx 5.61\ \mu_B$ and Weiss constant $\theta \approx -19$ K (Fig. 4b). However, the absence of any antiferromagnetic (AFM) ordering down to $T = 1.77$ K indicates that a high negative value of θ

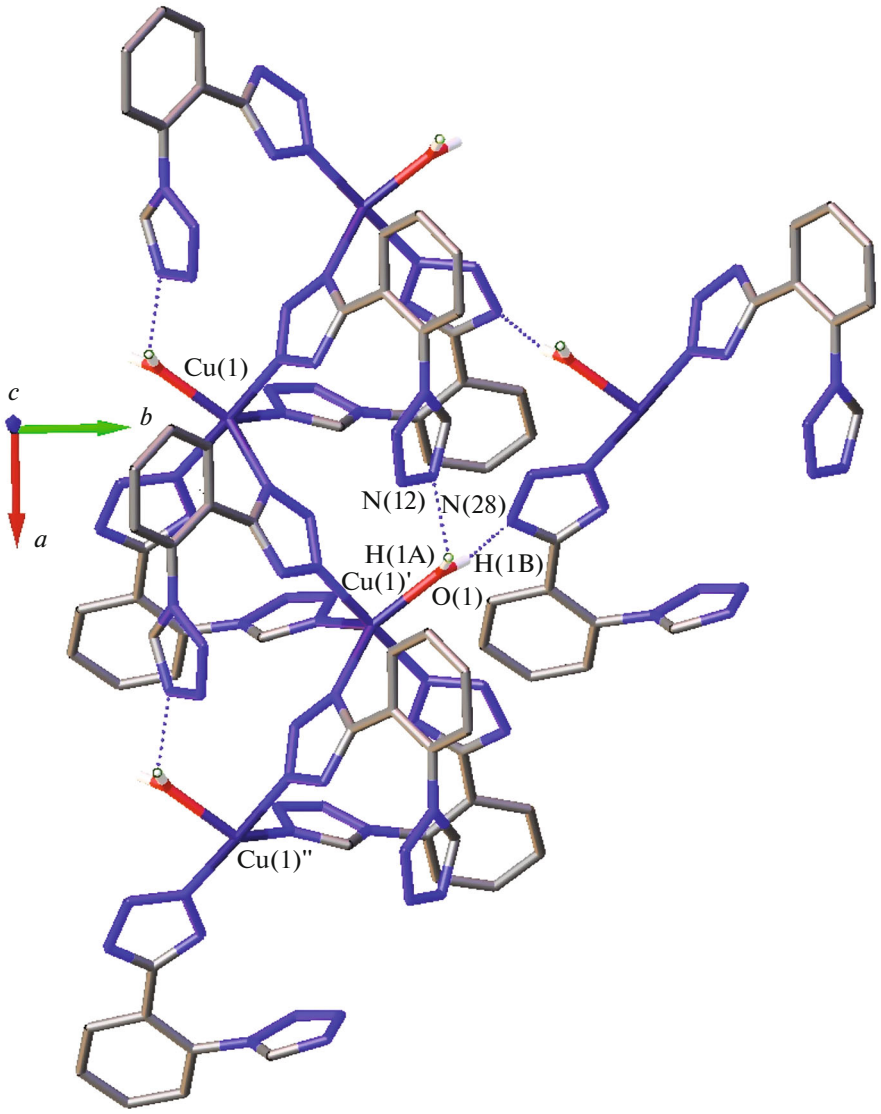

Fig. 3. Projection of the crystal structure of complex $[CuL_2(H_2O)]_n$ along the [001] direction.

obtained by this formal processing is not mainly related to exchange interactions but is induced by the temperature dependence $\mu_{eff}(T)$. The temperature dependence of the effective moment μ_{eff} (Fig. 4b) calculated for complex $[Co(HL)_2Cl_2]$ in the approximation of noninteracting moments ($\theta = 0$) is typical of the Co(II) complexes ($S = 3/2$), whose μ_{eff} decreases with decreasing temperature due to the splitting of the multiplet levels in the zero field and the g factor ($g \approx \mu_{eff}/1.94$) substantially exceeds 2 [30]. Undoubtedly, a decrease in μ_{eff} at low temperatures can also be induced by the AFM exchange interactions between the Co^{2+} ions, but it is difficult to reliably determine the value of this contribution, which is substantially weaker than the splitting of the levels in the zero field.

The magnetic behavior of the $[Cu(HL)_2Cl_2]$ and $[Cu(HL)_2Br_2]$ complexes was nontrivial. The magnetic susceptibility of the $[Cu(HL)_2Cl_2]$ complex is paramagnetic (Fig. 5a) and in the high-temperature range (30–300 K) can formally be described by the Curie–Weiss law with $\mu_{eff} \approx 1.87\ \mu_B$ and $\theta \approx -5.8$ K (Fig. 5b). The value of the effective moment corresponds to the expected values for the Cu^{2+} ions ($S = 1/2$) exceeding the spin-only value equal to $1.73\ \mu_B$ due to the contribution of orbital moments ($g \approx 2.16$). The obtained value of θ indicates substantial AFM exchange interactions. A more appropriate description of the chain crystal structure of the complexes can be obtained using the Bonner–Fisher dependence [31] proposed for AFM chains of ions with $S = 1/2$, whose interaction is expressed by the Hamiltonian

Table 3. Selected vibrational frequencies (cm^{-1}) in the spectra of HL and complexes **I–III**

HL	$[Co(HL)_2Cl_2]$	$[Cu(HL)_2Cl_2]$	$[Cu(HL)_2Br_2]$	Assignment
3264 br	3406 br	3204	3459 br	ν(NH)
		3147	3135	
3107	3135	3095	3010	ν(CH)
3078	3075	3076	2990	
1617	1612	1611	1613	R_{ring}
1576	1558	1554	1583	
1559	1507	1505	1529	
1506			1490	
	253	250	281	ν(M–N)
		230	247	
	325	294	216	ν(M–Hal)

$H = J\sum_i \vec{S}_i \cdot \vec{S}_{i+1}$. Indeed, the $\chi_p(T)$ data in a high-temperature range of 30–300 K are finely described by the Bonner–Fisher dependence with the parameters $J/k_B \approx 9$ K and $g \approx 2.16$ (orange dashed line in Figs. 5a, 5b). However, neither AFM transition expected for the three-dimensional network of exchange interactions, nor smooth maximum of the $\chi_p(T)$ dependence expected for AFM chains are observed at low temperatures. On the contrary, the magnetic susceptibility demonstrates a fast increase to a minimum achievable temperature of 1.77 K (Fig. 5a). The temperature dependence of the effective moment μ_{eff} calculated for complex $[Cu(HL)_2Cl_2]$ in the approximation of $\theta = 0$ (Fig. 5b) shows a pronounced inflection at ~14 K, where a decrease in μ_{eff} is changed by a fast increase.

In the case of competing interactions, the change in the interaction sign visible in the magnetic properties from the ferromagnetic (FM) interaction at high temperatures by AFM at low temperatures is a very frequent phenomenon: a stronger FM interaction in the magnetic sublattices and a weak AFM interaction between the sublattices is completed by the establishment of the AFM order. An opposite situation is pos-

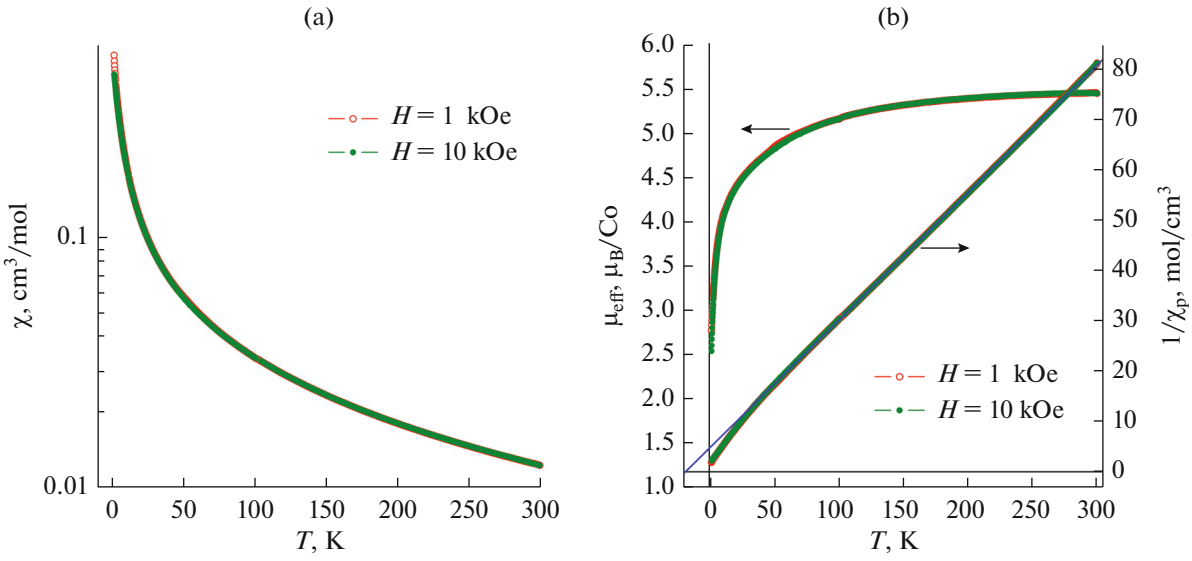

Fig. 4. Magnetic properties of complex $[Co(HL)_2Cl_2]$: (a) temperature dependences of the magnetic susceptibility χ measured in the magnetic field $H = 1$ and 10 kOe; (b) paramagnetic part of the temperature dependence of the susceptibility in the $1/\chi_p$ coordinates and the temperature dependence of μ_{eff} calculated in the approximation of noninteracting moments ($\theta = 0$; solid line shows the result of processing of the high-temperature part of the $1/\chi_p$ data according to the Curie–Weiss law at $\mu_{eff} = 5.61\ \mu_B$, $\theta = -19$ K).

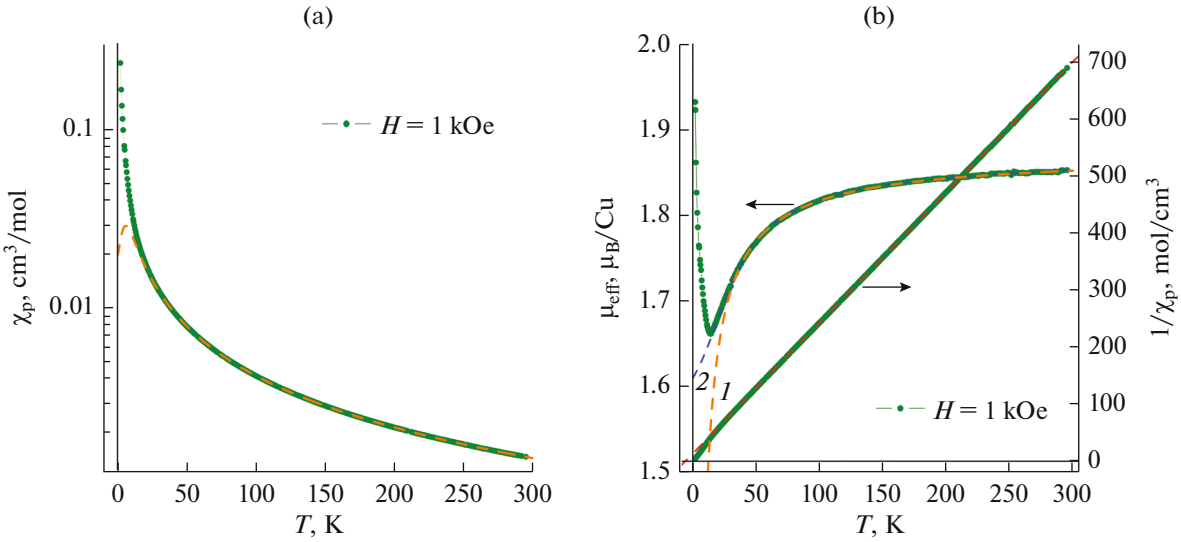

Fig. 5. Magnetic properties of complex $[Cu(HL)_2Cl_2]\cdot 0.5H_2O$: (a) temperature dependence of the magnetic susceptibility χ_p measured in the magnetic field $H = 1$ kOe (the Bonner–Fisher dependence [31] for chains of antiferromagnetically bound magnetic moments $S = 1/2$ ($J/k_B = 9$ K, $g = 2.16$) is shown by dash for comparison); (b) temperature dependence of $1/\chi_p$ (the result of processing of the high-temperature part of the $1/\chi_p$ data according to the Curie–Weiss law at $\mu_{eff} = 1.87\ \mu_B$ and $\theta = -5.8$ K is shown by red dashed line) and the temperature dependence of μ_{eff} calculated in the approximation of noninteracting moments ($\theta = 0$; (*1*) orange and (*2*) blue dashed lines are versions of the description of μ_{eff} on the basis of AFM chains, see text).

sible only in the form of weak ferromagnetism when the AFM sublattices are uncompensated or noncollinear. To check whether the low-temperature increase in the effective moment is a manifestation of weak ferromagnetism, we can analyze the field dependence of the magnetization, which is described by the equation, where $B_S(x)$ is the Brillouin function. An analysis of the experimental data on $M(H)$ shows (Fig. 6) that the magnetization at $H = 10$ kOe reaches 0.36 μ_B per copper ion and the functional dependence is closest to the behavior of the magnetic moments $S = 2$. This means that ferromagnetically ordered clusters containing, on the average, four Cu^{2+} ions each, are involved in magnetization at low temperatures rather than antiferromagnetically interacting moments. The extrapolation of the $M(H)$ curves to the range of high fields gives the saturation magnetization $M \sim 0.7\ \mu_B$/Cu. Taking into account quantum fluctuations, this means that at least ~75% copper ions are involved in FM correlations. This estimation excludes interpretations based on noncollinear AFM and ferromagnetic types of magnetic ordering, whose common property is low magnetization.

The nonmonotonic behavior of the $\mu_{eff}(T)$ dependence shown in Fig. 5b can be explained by two methods. First, the exchange interactions in the chains can change with decreasing temperature due to a change in the bond angles owing to which the AFM interaction between the Cu^{2+} ions with $J/k_B \approx 9$ K at high temperatures smoothly transforms into the FM interaction with $J/k_B \approx -0.8$ K at low temperatures. Second, AFM and FM polymer chains can coexist in the sample structure at all temperatures. The high-temperature behavior of $\mu_{eff}(T)$ can finely be described by a decreased (down to ≈25–26%) amount of AFM chains with a simultaneous increase in the exchange interaction in the chains to $J/k_B \approx 45$ K (blue dashed line in Fig. 5b). This amount of AFM chains does not contradict the data on the presence of ~75% FM chains at $T = 2$ K.

The observed features of the magnetic behavior are also reproduced for the $[Cu(HL)_2Br_2]$ complex with the only distinction that the g factor in this complex has a substantially higher value ($g \approx 2.46$) than that in its chloride-containing analog, and all interactions are shifted toward antiferromagnetism enhancement. In a high-temperature range of 50–300 K, the magnetic susceptibility of $\chi_p(T)$ can be described by the Bonner–Fisher dependence for AFM chains with the parameters $J/k_B \approx 22$ K and $g \approx 2.46$ (orange dashed lines in Figs. 7a, 7b). In the low-temperature range, the exchange interaction remains antiferromagnetic and weakens to $J/k_B \approx 2.3$ K. Similarly to $[Cu(HL)_2Cl_2]$, it is difficult to exclude a possibility of the coexistence in $[Cu(HL)_2Br_2]$ of two types of chains differed in the value of the intrachain AFM exchange interaction.

An analysis of all data obtained suggests that synthesized complexes **I**–**III** are polynuclear due to the coordination of two ligands HL by the nitrogen atoms of two tetrazole cycles to the adjacent metal ions. The coordination is supplemented to an octahedron by

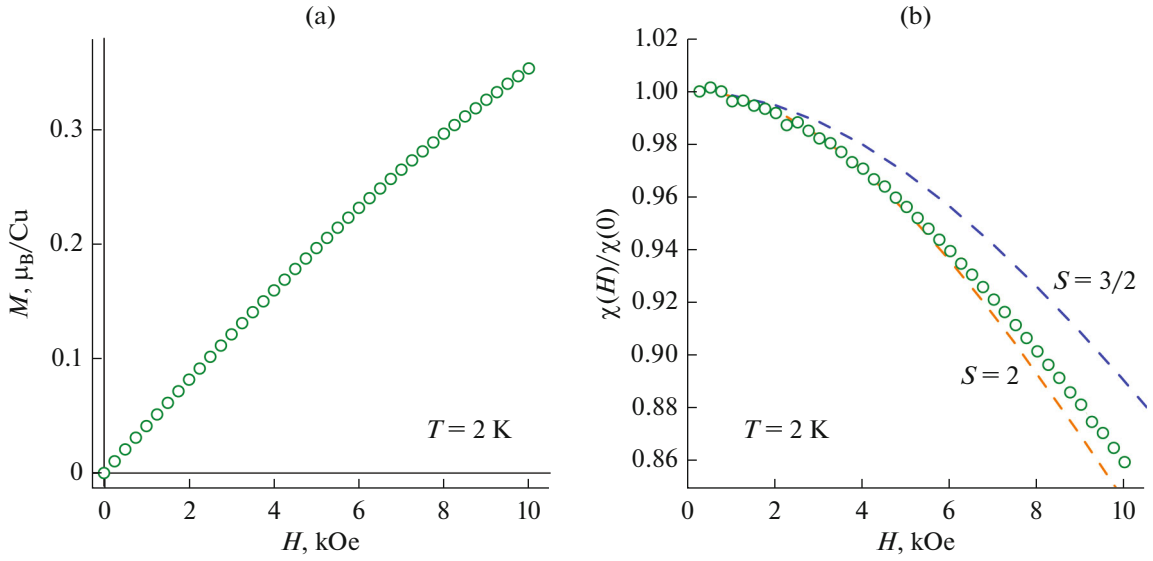

Fig. 6. Field dependences of the (a) magnetization M and (b) magnetic susceptibility $\chi = M/H$ for complex $[Cu(HL)_2Cl_2]\cdot 0.5H_2O$. The theoretical dependences based on the Brillouin function for the magnetic moments $S = 3/2$ and $S = 2$ are shown by dashed lines (Fig. 6a).

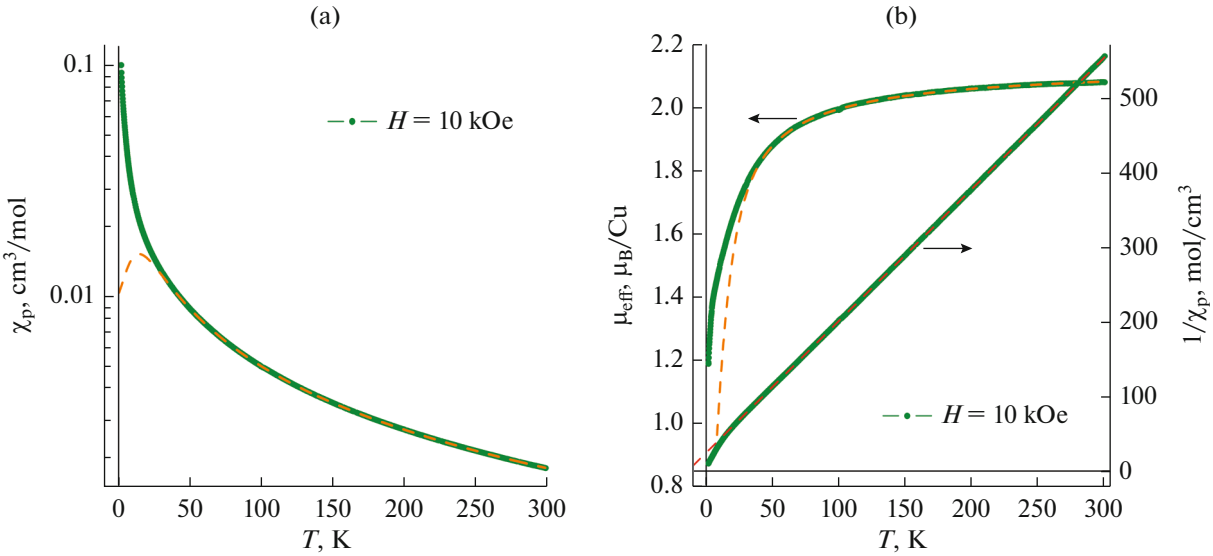

Fig. 7. Magnetic properties of complex $[Cu(HL)_2Br_2]$: (a) temperature dependences of the magnetic susceptibility χ_p measured in the magnetic field $H = 10$ kOe (the Bonner–Fisher dependence for AFM chains at $J/k_B = 22$ K, $g = 2.46$) is shown by dashed line); (b) paramagnetic part of the temperature dependence of the susceptibility in the $1/\chi_p$ coordinates and the temperature dependence of μ_{eff} calculated in the approximation of noninteracting moments ($\theta = 0$; the result of processing of the high-temperature part of the $1/\chi_p$ data according to the Curie–Weiss law at $\mu_{eff} = 2.13\ \mu_B$ and $\theta = -14.5$ K is shown by red dashed line, and the description based on AFM chains (see text) is shown by orange dashed line).

halide ions (coordination nodes MN_4Hal_2 (Hal = Cl^-, Br^-)).

Thus, the Co(II) and Cu(II) coordination compounds with the new ligand, 5-(2-(1*H*-tetrazol-1-yl)phenyl)-1*H*-tetrazole, were synthesized and studied. The crystal structure of the polynuclear copper(II) complex with 5-(2-(1*H*-tetrazol-1-yl)phenyl)-1*H*-tetrazolate $[CuL_2(H_2O)]_n$ was determined by XRD. The magnetic studies show that the magnetic properties of the Co(II) complex are mainly determined by a strong splitting of the levels in the zero field. The magnetic susceptibility of the copper(II) complexes can be described in terms of one-dimensional chains of the Cu^{2+} ions, the exchange interac-

tion J/k_B in which changes with decreasing temperature from ≈ +9 K (AFM) to ≈ –0.8 K (FM) for $[Cu(HL)_2Cl_2]$ and from ≈ +22 to +2.3 K for the $[Cu(HL)_2Br_2]$ complex. An alternative version of the description is the coexistence in the copper complexes of two types of chains with different values of the exchange interaction.

ACKNOWLEDGMENTS

The authors are grateful to A.O. Matveev for recording XRD patterns, A.S. Sukhikh for single-crystal XRD experiment, L.A. Sheludyakov for recording IR spectra, and I.V. Yushin for recording diffuse reflectance spectra.

FUNDING

This work was supported by the Russian Science Foundation (project no. 20-63-46026, magnetic properties) and Ministry of Science and Higher Education of the Russian Federation (projects nos. 121031700313-8 and 21031700314-5, synthesis and structure).

CONFLICT OF INTEREST

The authors declare that they have no conflicts of interest.

REFERENCES

1. Yang, G.W., Zhang, Y.T., Wu, Q., et al., *Inorg. Chim. Acta*, 2016, vol. 450, p. 364.
2. Wright, P.J., Kolanowski, J.L., Filipek, W.K., et al., *Eur. J. Inorg. Chem.*, 2017, p. 5260.
3. Kaleeswaran, P., Azath, I.A., Tharmaraj, V., et al., *ChemPlusChem*, 2014, vol. 79, p. 1361.
4. Xing, G., Zhang, Y., and Cao, X., *J. Mol. Struct.*, 2017, vol. 1146, p. 793.
5. Nasani, R., Saha, M., Mobin, S.M., et al., *Dalton Trans.*, 2014, vol. 43, p. 9944.
6. Wang, F., Zhang, J., Yu, R., et al., *CrystEngComm*, 2010, vol. 12, p. 671.
7. Tao, P., Zhang, Y., Wang, J., et al., *J. Mater. Chem. C*, 2017, vol. 5, p. 9306.
8. Umamahesh, B., Karthikeyan, N.S., Sathiyanarayanan, K.I., et al., *J. Mater. Chem. C*, 2016, vol. 4, p. 10053.
9. Colombo, A., Dragonetti, C., Magni, M., et al., *Dalton Trans.*, 2015, vol. 44, p. 11788.
10. Xu, R.-J., Fu, D.-W., Dai, J., et al., *Inorg. Chem. Commun.*, 2011, vol. 14, p. 1093.
11. Gaponik, P.N., Voitekhovich, S.V., and Ivashkevich, O.A., *Russ. Chem. Rev.*, 2006, vol. 75, no. 6, p. 507. https://doi.org/10.1070/RC2006v075n06ABEH003601
12. Zhao, H., Qu, Z.-R., Ye, H.-Y., et al., *Chem Soc. Rev.*, 2008, vol. 37, p. 84.
13. Ouellette, W., Jones, S., and Zubieta, J., *CrystEngComm*, 2011, vol. 13, p. 4457.
14. Kang, X.-M., Tang, M.-H., Yang, G.-L., et al., *Coord. Chem. Rev.*, 2020, vol. 422, p. 213424.
15. Chi, Y., Tong, B., and Chou, P.-T., *Coord. Chem. Rev.*, 2014, vol. 281, p. 1.
16. Massi, M., Stagni, S., and Ogden, M.I., *Coord. Chem. Rev.*, 2017, vol. 375, p. 164.
17. Shakirova, O.G., Lavrenova, L.G., Kuratieva, N.V., et al., *J. Struct. Chem.*, 2017, vol. 58, no. 5, p. 919. https://doi.org/10.1134/S0022476617050092
18. Grigorieva, I.M., Serebryanskaya, T.V., Grigoriev, Y.V., et al., *Polyhedron*, 2018, vol. 151, p. 74.
19. Voitekhovich, S.V., Grigoriev, Yu.V., Lyakhov, A.S., et al., *Polyhedron*, 2020, vol. 176, p. 114299.
20. Ivanova, A.D., Grigoriev, Yu.V., Komarov, V.Yu., et al., *Polyhedron*, 2020, vol. 189, p. 114750.
21. Ivanova, A.D., Grigoriev, Yu.V., Komarov, V.Yu., et al., *Inorg. Chim. Acta*, 2021, vol. 524, p. 120452.
22. Voitekhovich, S.V., Grigoriev, Yu.V., Lyakhov, A.S., et al., *Polyhedron*, 2021, vol. 194, p. 114907.
23. *Bruker APEX3 Software Suite (APEX3 v.2019.1-0, SADABS v. 2016/2, SAINT v. 8.40a)*, Madison: Bruker Nonius (2003–2004), Bruker AXS (2005–2018), Bruker Nano (2019).
24. Sheldrick, G.M., *Acta Crystallogr., Sect. A: Found. Adv.*, 2015, vol. 71, p. 3.
25. Sheldrick, G.M., *Acta Crystallogr., Sect. C: Struct. Chem.*, 2015, vol. 71, p. 3.
26. Dolomanov, O.V., Bourhis, L.J., Gildea, R.J., et al., *J. Appl. Crystallogr.*, 2009, vol. 42, p. 339.
27. Butler, R.N., in *Comprehensive Heterocyclic Chemistry*, Katritzky, A.R. and Rees, C.W., Eds., Oxford.: Pergamon, 1984, vol. 5, p. 791.
28. Gaponik, P.N., Karavai, V.P., and Grigoriev, Yu.V., *Chem. Heterocycl. Compd.*, 1985, vol. 21, no. 11, p. 1255.
29. Grigoriev, Yu.V., Voitekhovich, S.V., Karavai, V.P., et al., *Chem. Heterocycl. Compd.*, 2017, vol. 53, nos. 6–7, p. 670. https://doi.org/10.1007/s10593-017-2108-7
30. Boča, R., *Coord. Chem. Rev.*, 2004, vol. 248, p. 757.
31. Bonner, J.C. and Fisher, M.E., *Phys. Rev.*, 1964, vol. 135, p. A640.

Translated by E. Yablonskaya